Magnetization and heat-capacity measurements on $Zn_{1-x}Cr_xTe$

T. M. Pekarek, J. E. Luning,* I. Miotkowski, and B. C. Crooker
Department of Physics, Purdue University, West Lafayette, Indiana 47907
(Received 29 July 1994; revised manuscript received 12 September 1994)

We have taken magnetization and calorimetric measurements on $Zn_{1-x}Cr_xTe$ ($x=0.003$). The heat-capacity measurements show a Schottky peak indicating an energy-level splitting of 3.1 K between the ground and first excited states. Above 1.5 K we observe additional heat capacity, which indicates the presence of additional low-energy vibronic excitations. The magnetization data reveal a small anisotropy ($\sim 7\%$) with the (111) direction giving the largest value. The magnetization data were fit with a model including a static Jahn-Teller distortion proposed previously in these materials [J. T. Vallin, G. A. Slack, S. Roberts, and A. E. Hughes, Phys. Rev. B **2**, 4313 (1970)]. Reasonable agreement was found with the data for a spin-orbit parameter of $-59\ cm^{-1}$ and a Jahn-Teller energy of $320\ cm^{-1}$.

I. INTRODUCTION

The class of alloys known as diluted magnetic semiconductors[1] (DMS's) take the form $A_{1-x}M_xB$ where M is a transition-metal ion and A and B are elements from the second and sixth column of the Periodic Table, respectively. A substantial amount is known about Mn-based DMS's and somewhat less about Co and Fe-based alloys. $A_{1-x}Cr_xB$ materials, on the other hand, have received less attention. Some earlier optical-absorption,[2-5] luminescence,[6] and electron-paramagnetic-resonance[7] (EPR) experiments have been reported on II-IV semiconductor crystals with a low concentration of Cr.

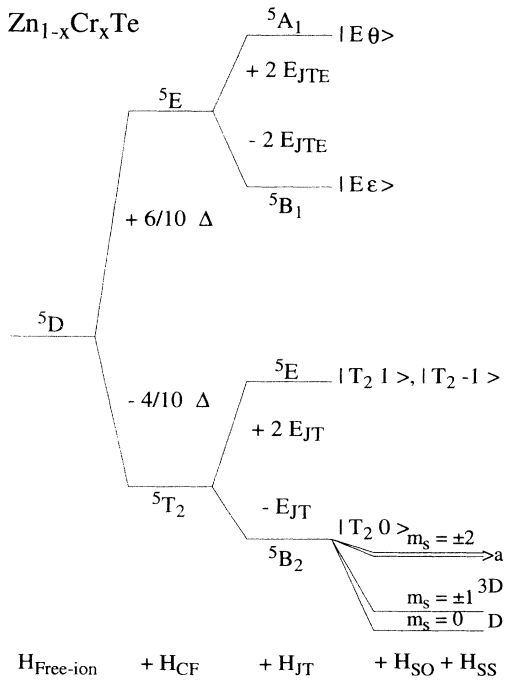

FIG. 1. Energy-level splittings for the $3d$ electrons of Cr^{2+} in ZnTe including crystal-field, Jahn-Teller, spin-orbit, and spin-spin effects.

Based on this experimental work, Vallin *et al.* suggested that there is a static Jahn-Teller distortion in Cr^{2+}-based DMS's.[2] This results in a static displacement of the Cr^{2+} ion from its lattice site along one of three equivalent directions along the (100), (010), or (001) cubic axes. The symmetry is lowered, the energy states are split, and the total energy of the system decreases. Shown in Fig. 1 is the splitting for Cr^{2+} in DMS's of T_d symmetry with a tetragonal Jahn-Teller distortion. The key feature is an orbital singlet, $S=2$ ground-state multiplet with a small splitting of the m_s states.

Recently, interest in the chromium-based DMS's has increased with the publication of several theoretical[8-11] and experimental[12,13] papers. The key difference between chromium and the previously studied transition metals (Mn, Fe, Co) arises from the nature of the exchange interaction between the valence band p-type electrons and the d electrons of the transition metal. This interaction, which involves p-d hybridization, is predominantly due to d electrons with t-type symmetry. In the case of Mn, Fe, and Co the spin-up t orbitals are occupied and the spin-down t orbitals are empty. In the case of Cr^{2+}, only two of the three spin-up t orbitals are occupied, leading to new exchange channels. The recent observation of ferromagnetic p-d exchange in a chromium-based DMS (Ref. 13) was argued to result from these new exchange channels. The theory of Bhattacharjee[11] also suggests that $Cd_{1-x}Cr_xTe$ and $Zn_{1-x}Cr_xTe$ will show large magneto-optical effects due to the close proximity of the chromium donor level with t-type symmetry to the top of the valence band.[14]

In this paper we present magnetization, and heat-capacity data measured on bulk $Zn_{1-x}Cr_xTe$ crystals grown from the melt. Using the model Hamiltonian of Vallin *et al.* we numerically diagonalize the resulting 25×25 matrix and compare the predicted magnetization to our data.

II. EXPERIMENTAL DETAILS

Single-crystal $Zn_{1-x}Cr_xTe$ samples were grown by the vertical Bridgman method. In this work we report on

two samples, A and B, cut from a single boule with nominal Cr^{2+} concentration $x=0.005$. Sample A was used for the magnetization measurements and sample B was used for the heat-capacity measurements. Typically, the actual concentration is somewhat less than the nominal value in samples grown by this method. Atomic absorption spectroscopy (AAS) was performed on small chips taken from samples A and B yielding values of $x=0.0035\pm0.0005$ and $x=0.0019\pm0.0004$, respectively. The ratio of saturation magnetization values for the two samples and the concentration determined by a Schottky fit to the specific heat data from sample B were consistent with these concentrations.

Magnetization data were taken on a Cryogenic Consultants Limited SQUID magnetometer for fields between 0 and 6 T and temperatures between 1.5 and 300 K. Samples were oriented along the (111), (110), and (100) directions by the standard Laue diffraction technique. The samples exhibited a hysteresis loop at low fields revealing the presence of a ferromagnetic minority phase.[15] The ferromagnetic signal saturates by about 0.5 T at low temperatures with a magnitude of 0.055 emu/g (Fig. 2). Magnetization measurements as a function of temperature suggest a Curie temperature slightly above 300 K for the minority phase.

Both the diamagnetic signal from the ZnTe and the ferromagnetic signal from this minority phase were subtracted from the data. We report only magnetization data above 1 T where the ferromagnetic signal is saturated. The saturation value is obtained from measurements of the hysteresis loop and its temperature dependence was fit to the standard low-temperature ferromagnetic behavior: $M=M_{\rm sat}\,(1-AT^{3/2})$, where A is a positive constant.

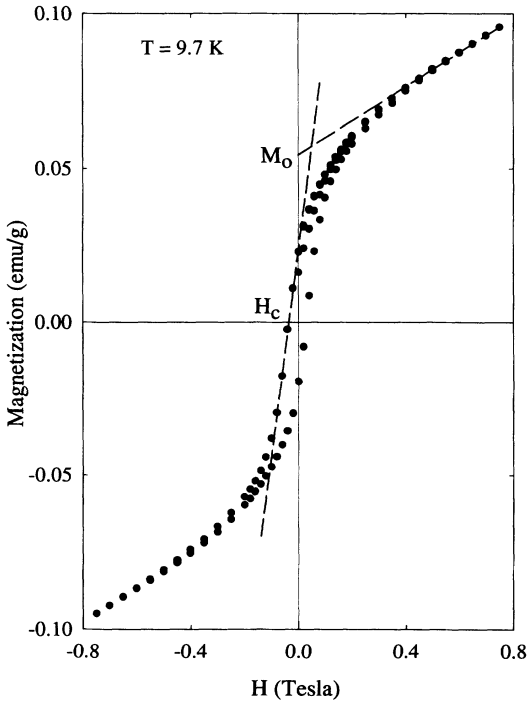

FIG. 2. Hysteresis loop showing a ferromagnetic minority phase. The saturated magnetization of this ferromagnetic inclusion is M_0 and the coercive field is H_c. The signal is believed to be due to CrTe. The diamagnetic contribution has been subtracted.

Heat-capacity data were measured on a 0.58 g sample in a pumped ^{3}He cryostat using the quasiadiabatic heat-pulse method. Measurements were taken between 0.4 and 5 K in zero field. Both the addenda corrections and the lattice contribution from the ZnTe were subtracted leaving a residual heat capacity, which we attribute to the Cr^{2+} in our sample. In the region of the Schottky peak at 1 K, this residual accounts for roughly 80% of the total observed heat capacity.

III. THEORETICAL MODEL

In the analysis of our results, we utilized a model proposed by Vallin and Watkins[7] for the $3d$ states of Cr^{2+} in $Zn_{1-x}Cr_xTe$, which includes the crystal-field, Jahn-Teller, spin-orbit, spin-spin, and Zeeman effects as well as ligand admixture corrections. We constructed the full 25×25 matrix for the Cr^{2+}, which was numerically diagonalized to yield the energy levels as a function of field. These were then used to calculate the magnetization as a function of field and temperature.

The crystal-field environment of the Cr^{2+} in the host ZnTe has tetrahedral (T_d) symmetry, which can be written in terms of operator equivalents for $L=2$ as[16,17]

$$H_{\rm CF}(T_d)=\frac{\Delta}{10}\left[\tfrac{1}{8}(L_+^2+L_-^2)^2+\tfrac{3}{2}L_z^4-6L_z^2-\tfrac{12}{5}\right], \tag{1}$$

where Δ is the crystal-field splitting parameter. This reduces to diagonal form for the basis states[18]

$$\begin{aligned}
&{}^5E:\ {}^5A_1:\ |E\theta\rangle=|0\rangle\ ,\\
&\qquad {}^5B_1:\ |E\varepsilon\rangle=\frac{1}{\sqrt{2}}(|2\rangle+|-2\rangle)\ ;\\
&{}^5T_2:\ {}^5E:\ |T_2 1\rangle=|-1\rangle\ ,\\
&\qquad\qquad |T_2-1\rangle=-|1\rangle\ ,\\
&\qquad {}^5B_2:\ |T_2 0\rangle=\frac{1}{\sqrt{2}}(|2\rangle-|-2\rangle)\ .
\end{aligned} \tag{2}$$

As shown in Fig. 1, the crystal-field splits the d electronic states into an orbital doublet (^5E) and a lower lying orbital triplet ($^5T_2$).

The static Jahn-Teller distortion of the Cr^{2+} ion off of its lattice site is driven by mixing the E phonon mode with the ^5E and the $^5T_2$ electronic states according to[2,19,20]

$$\begin{aligned}
H_{\rm JT}=&V_1(Q_\theta \mathbf{E}_\theta+Q_\varepsilon \mathbf{E}_\varepsilon)+V_2(Q_\theta \mathbf{U}_\theta+Q_\varepsilon \mathbf{U}_\varepsilon)\\
&+\tfrac{1}{2}\kappa(Q_\theta^2+Q_\varepsilon^2)\ ,
\end{aligned} \tag{3}$$

where V_1 and V_2 are the coupling coefficients between the lattice and the $^5T_2$ and ^5E states, respectively. The last term is the potential energy of the distorted lattice where $\kappa=\mu\bar{\omega}^2$ is the elastic lattice constant, μ is the ion mass, and $\bar{\omega}$ is the phonon frequency. Q_θ and Q_ε are the nuclear displacements. The electronic operators for $^5T_2$

are $\mathbf{E}_\theta$ and $\mathbf{E}_\varepsilon$ and for ^5E are $\mathbf{U}_\theta$ and $\mathbf{U}_\varepsilon$. This term is also diagonal for our choice of electronic basis states and yields ground-state minima for the nuclear displacements,

$$Q_\theta=\frac{V_1}{\kappa}\ , \quad \text{and } Q_\varepsilon=0\ ,$$
$$Q_\theta=-\frac{V_1}{\kappa}\ , \quad \text{and } Q_\varepsilon=\sqrt{3}\frac{V_1}{2\kappa}\ , \tag{4}$$

or

$$Q_\theta=-\frac{V_1}{\kappa}\ , \quad \text{and } Q_\varepsilon=-\sqrt{3}\frac{V_1}{2\kappa}\ .$$

Each of these three equivalent static distortions along the (100), (010), and (001) directions results in an orbital singlet ($^5B_2$) with an energy $E_{\rm JT}=V_1^2/2\kappa$ below the $^5T_2$ state and a doublet (^5E) with an energy $2E_{\rm JT}$ above the $^5T_2$ state (Fig. 1). The symmetry is reduced from T_d to D_{2d}. This static distortion also leads to a splitting of the ^5E state into the orbital singlets $^5A_1$ and $^5B_1$, due to the term $V_2(Q_\theta\mathbf{U}_\theta+Q_\varepsilon\mathbf{U}_\varepsilon)$. As shown in Fig. 1, the ^5E state is split by $4E_{JTE}$,where $E_{JTE}=V_2^2/2\kappa=\eta^2E_{\rm JT}$ and $\eta=V_2/V_1$.

The point-ion treatment of the spin-orbit, spin-spin, and Zeeman interactions take their usual form,

$$H_{\rm SO}=\lambda(\mathbf{L}\cdot\mathbf{S})\ ,$$
$$H_{\rm SS}=-\rho[(\mathbf{L}\cdot\mathbf{S})^2+\tfrac{1}{2}(\mathbf{L}\cdot\mathbf{S})-\tfrac{1}{3}L(L+1)S(S+1)]\ , \tag{5}$$

and

$$H_B=\mu_B(\mathbf{L}+2\mathbf{S})\cdot\mathbf{B}\ .$$

Here, λ and ρ are the spin-orbit and spin-spin parameters, respectively, and μ_B is the Bohr magneton. However, in addition to the crystal-field splitting due to a point-ion analysis of the crystal environment of the Cr^{2+}, the chemical bonds, themselves, have been shown to have an important effect on the energy levels of the Cr^{2+} ion.[7] Since the chemical bonding between ions perturbs the p electronic states into σ and π bonds, the p states and the magnetic d states are no longer perfectly orthogonal. Their nonzero overlap contributes to the effective spin-orbit and spin-spin parameters.

The addition of ligand-field terms requires four different ρ's and three λ's, which act on different regions of the complete 25×25 matrix. Within the ^5E multiplet we have

$$H_{\rm SO}=\lambda(\mathbf{L}\cdot\mathbf{S})\ ,$$
and
$$H_{\rm SS}=-\rho[(\mathbf{L}\cdot\mathbf{S})^2+\tfrac{1}{2}(\mathbf{L}\cdot\mathbf{S})-\tfrac{1}{3}L(L+1)S(S+1)]\ . \tag{6}$$

Since the results depend only weakly on the ^5E levels, we use the free ion values of $\rho=0.12\ \text{cm}^{-1}$ and $\lambda=57\ \text{cm}^{-1}$ for these terms. For coupling between the ^5E and $^5T_2$ multiplets we have

$$H_{\rm SO}=\lambda_2(\mathbf{L}\cdot\mathbf{S})\ ,$$
and
$$H_{\rm SS}=-\rho_2[(\mathbf{L}\cdot\mathbf{S})^2+\tfrac{1}{2}(\mathbf{L}\cdot\mathbf{S})-\tfrac{1}{3}L(L+1)S(S+1)]\ . \tag{7}$$

Within these regions, the interactions have only E symmetry so each region needs only a single λ and ρ.

Within the ground $^5T_2$ multiplet, however, the spin-spin interaction can have terms with E or T_2 symmetry. Therefore, the spin-spin Hamiltonian must be rewritten in the form

$$H_{\rm SS}=-\tfrac{2}{3}\rho_1(\mathbf{L}_\theta\mathbf{S}_\theta+\mathbf{L}_\varepsilon\mathbf{S}_\varepsilon)-\tfrac{1}{2}\rho_3(\mathbf{L}_\xi\mathbf{S}_\xi+\mathbf{L}_\eta\mathbf{S}_\eta+\mathbf{L}_\zeta\mathbf{S}_\zeta)\ , \tag{8}$$

where ρ_1 accounts for interactions with E symmetry, ρ_3 accounts for interactions with T_2 symmetry, and

$$\mathbf{L}_\theta=\mathbf{L}_z^2-\tfrac{1}{2}(\mathbf{L}_x^2+\mathbf{L}_y^2)\ ,$$
$$\mathbf{L}_\varepsilon=\frac{\sqrt{3}}{2}(\mathbf{L}_x^2-\mathbf{L}_y^2)\ ,$$
$$\mathbf{L}_\xi=\mathbf{L}_y\mathbf{L}_z+\mathbf{L}_z\mathbf{L}_y\ , \tag{9}$$
$$\mathbf{L}_\eta=\mathbf{L}_z\mathbf{L}_x+\mathbf{L}_x\mathbf{L}_z\ ,$$

and

$$\mathbf{L}_\zeta=\mathbf{L}_x\mathbf{L}_y+\mathbf{L}_y\mathbf{L}_x\ ,$$

with corresponding expression for $\mathbf{S}_\theta$, $\mathbf{S}_\varepsilon$, $\mathbf{S}_\xi$, $\mathbf{S}_\eta$, and $\mathbf{S}_\zeta$. Finally, the spin-orbit Hamiltonian within the ground $^5T_2$ multiplet is given by

$$H_{\rm SO}=\lambda_1(\mathbf{L}\cdot\mathbf{S})\ . \tag{10}$$

These five effective spin-orbit and spin-spin parameters including ligand admixture corrections can all be written in terms of the free-ion values plus two additional parameters,

$$\lambda_1\cong\lambda(1-K)\ ,$$
$$\lambda_2\cong\lambda\left[1-\frac{K}{8}\right]\ ,$$
$$\rho_1=\frac{5}{9E}(\lambda_1^2+2\lambda_2^2)+\rho\ , \tag{11}$$
$$\rho_2=\frac{5}{3E}\lambda_1\lambda_2+\rho\ ,$$

and

$$\rho_3=\frac{5}{9E}(-\lambda_1^2+4\lambda_2^2)+\rho\ .$$

The parameter K sets the overall magnitude of the mixing with the σ and π bonds. The spin-spin corrections arise from mixing with the next highest LS state of the same symmetry ($3d^4$) which has $L=2$ and $S=1$. This state is at an energy $E\cong20\,000\ \text{cm}^{-1}$ above the $L=S=2$ ground state. Note that in the absence of any mixing with the σ and π bonds, $K=0$, and $\lambda_1=\lambda_2=\lambda$ and $\rho_1=\rho_2=\rho_3=(5/3E)\lambda^2+\rho$. And, in the limit where the next highest LS state is increasingly further away ($E\to\infty$), $\rho_1=\rho_2=\rho_3=\rho$.

This system is then fully described by five parameters: Δ, $E_{\rm JT}$, E_{JTE}, K, and E. All of these parameters can be determined from previous work. E is taken as $20\,000\ \text{cm}^{-1}$,[7] although the system is relatively insensitive to

reasonable deviations from this value. E_{JT} has been directly measured by infrared absorption to be 320 cm^{-1}.[5] The parameters Δ and E_{JTE} can be determined by combining this measurement of E_{JT} with the near-infrared absorption measurements of the zero-phonon energy E_{ZP} and the peak phonon energy E_{peak} by[2]

$$\Delta = E_{ZP} - (1-\eta^2)E_{JT} \ , \quad \text{and} \quad E_{JTE} = \eta^2 E_{JT} \ , \tag{12}$$

where

$$\eta = -1 + \left[\frac{E_{peak} - E_{ZP}}{E_{JT}} \right]^{1/2} . \tag{13}$$

The values of E_{ZP} and E_{peak} are taken from the near-infrared absorption data to be $E_{ZP}=4994$ cm^{-1} and $E_{peak}=5530$ cm^{-1}.[2] From this we obtain $\Delta=4700$ cm^{-1}, $E_{JTE}=30$ cm^{-1}, and $\eta=0.294$. Alternately, the value of E_{JTE} was measured to be 40 cm^{-1} from absorption and luminescence measurements.[5] However, the structure in this last spectra has also been interpreted as arising from phonon modes rather than the E_{JTE} splitting.[20]

With set vlaues for Δ, E_{JT}, E_{JTE}, and E, the value of K is obtained from the value of D as determined by the electron-spin-resonance results and our heat-capacity measurement. With $D=3.1$ K, we find K=2.04. This results in effective spin-orbit and spin-spin parameters of $\lambda_1=-59.4$ cm^{-1}, $\lambda_2=42.4$ cm^{-1}, $\rho_1=0.32$ cm^{-1}, $\rho_2=-0.09$ cm^{-1}, and $\rho_3=0.22$ cm^{-1} for $Zn_{1-x}Cr_xTe$. We note that our values for these parameters are different from those reported previously by Vallin and coworkers[5,7] who assumed $E_{JTE}=0.0$ cm^{-1} in their calculations.

With the system reduced to zero adjustable parameters, we calculated the energy levels for $Zn_{1-x}Cr_xTe$ as a function of field. Shown in Figs. 3(a), 3(b), 3(c), and 3(d) are the energy levels for a Jahn-Teller distortion along the (001) direction and an externally applied magnetic field along the (001), (111), (1m0), and (011) directions, respectively.

IV. EXPERIMENTAL RESULTS

A. Heat capacity

The excess heat capacity for $Zn_{1-x}Cr_xTe$ after subtraction of the lattice contribution is shown in Fig. 4. The exponential decrease in the heat capacity at low temperatures is typical of a Schottky peak. From the theory[5] we expect a ground-state multiplet consisting of an $m_s=0$ ground state with a degenerate $m_s=\pm1$ level a distance D above, and a nearly degenerate $m_s=\pm2$ levels a distance $4D$ above.

The data was fit with a three-level Schottky peak, shown in Fig. 4 as a solid line. From the fit we obtain a value of $D=3.1\pm0.1$ K ($=2.15$ cm^{-1}). This result is in

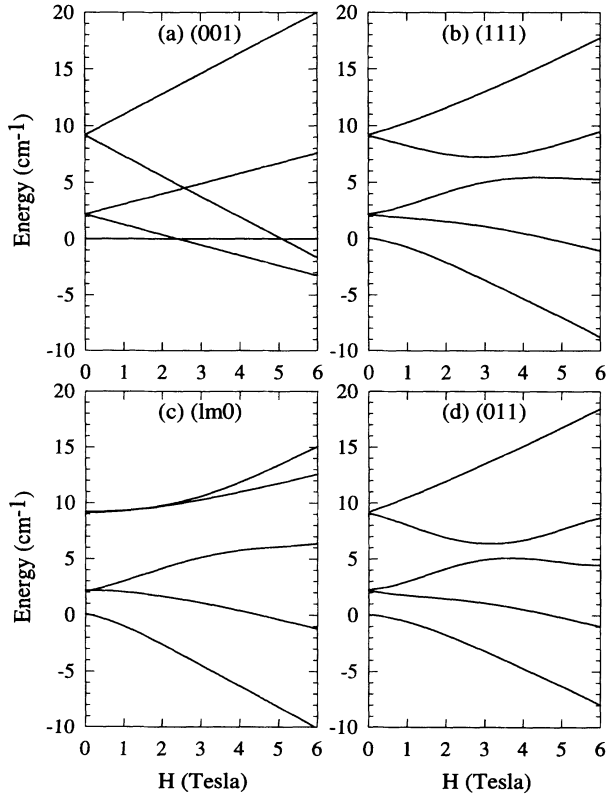

FIG. 3. Energy levels for the ground-state multiplet for Cr^{2+} in ZnTe. The field and orientational dependence of the energy levels were calculated by numerically solving the 25×25 Hamiltonian for the ^5D state.

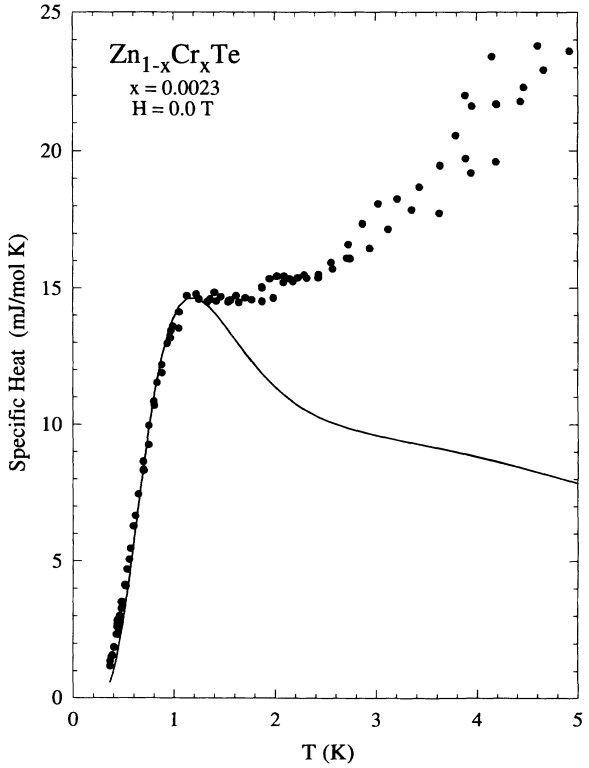

FIG. 4. Heat-capacity data for $Zn_{1-x}Cr_xTe$ with a theoretical three-level Schottky peak shown as a solid line. The rise in the heat capacity above the Schottky peak for $T>1.5$ K is discussed in the text.

good agreement with the value reported from electron-spin-resonance measurements of 2.30 ± 0.17 cm^{-1}.[5] We also obtain a value for the Cr concentration of $x=0.0023\pm^{0.00005}_{0.0005}$, in agreement with the AAS results and the magnitude of the saturated magnetization.

As can be seen, the agreement between the calculated Schottky peak and the data is good from low temperatures through the peak. Above the peak the data show a large excess. Similar excess heat capacity has also been observed in $Zn_{1-x}Cr_xSe$.[12] We believe this excess heat capacity is related to the abrupt broadening of the EPR linewidth above ~7 K for $Zn_{1-x}Cr_xTe$ and ~8 K for $Zn_{1-x}Cr_xSe$ (Ref. 7) and to the structure observed in luminescence spectra.[5,6,21] The luminescence spectra have been interpreted in terms of several broad vibronic energy bands, the lowest of which is centered at 60 cm^{-1} in ZnS (Ref. 6) and 52 cm^{-1} in ZnSe.[21] This additional structure in the phonon spectrum arises from the Jahn-Teller induced displacement of the Cr^{2+} atoms from the normal lattice sites. It seems likely that the sharp rise in heat capacity that we observe arises from these vibronic energy bands.

B. Magnetization

The magnetization of $Zn_{1-x}Cr_xTe$ as a function of field at 3.67 K is shown in Fig. 5 for three orientations. The magnetization grows slower than a standard Brillouin function and more rapidly then a Van Vleck system

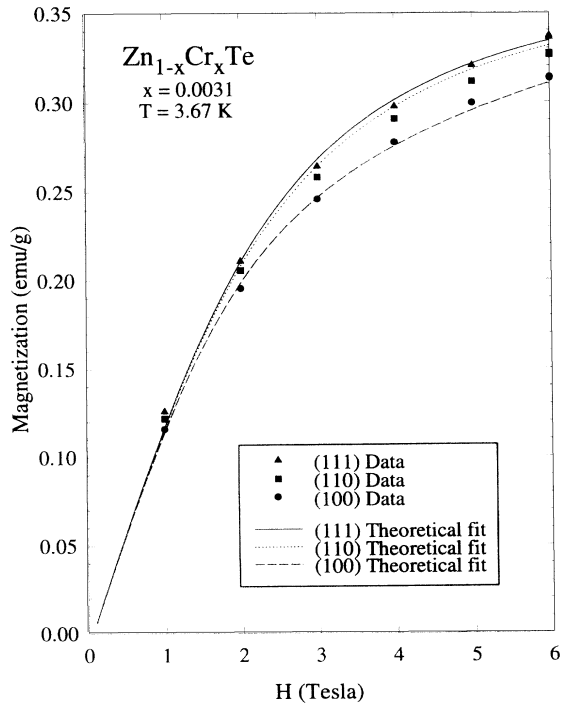

FIG. 5. Magnetization data for $Zn_{1-x}Cr_xTe$ with a theoretical fit including a static tetragonal Jahn-Teller distortion and ligand-field corrections to λ and ρ. An anisotropy in the magnetization is evident. The ferromagnetic and diamagnetic contributions have been subtracted.

indicating that the lowest multiplet has a small splitting. By 6.0 T, the magnetization is approaching saturation. From Fig. 5 we estimate a saturated value of ~0.36 emu/g. Using the value of concentration $x=0.0035\pm0.005$ obtained from AAS, we obtain an effective Cr^{2+} moment of $p=3.6\pm0.5\mu_B$. This is close to the expected value of 4.0 for a pure spin two system. The magnetization is anisotropic with the (111) direction having the largest value. The anisotropy splitting is ~7% of the total signal by 6.0 T. Similar measurements were taken at 2.0 and 5.4 K (not shown) and displayed similar behavior.

The magnetization vs field curves for several orientations were obtained using the energy levels for the Cr^{2+} ground multiplet calculated numerically from the 25×25 Hamiltonian (Fig. 3). The results are plotted as a set of three lines in Fig. 5. The concentration, $x=0.0031$, was chosen to give the correct magnetization at 6.0 T and is in agreement with the AAS results.

In our analysis we have assumed that the Jahn-Teller distortions are frozen and randomly distributed along the three equivalent crystalline axes. For a magnetic field along the (100) direction, for example, $\frac{1}{3}$ of the Cr^{2+} ions will have their Jahn-Teller distortion along the field direction. The energy levels for these atoms will be as shown in Fig. 3(a). The remaining $\frac{2}{3}$ of the Cr^{2+} ions will have their Jahn-Teller distortion perpendicular to the field direction and will have energy levels shown in Fig. 3(c).

The theory with frozen Jahn-Teller distortions correctly predicts both the initial slope and anisotropy with the (111) direction having the greatest magnetization. Further, the magnitude of the anisotropy splitting is correctly predicted. The small discrepancies between the calculated and experimental magnetization may result from small strain- or field-induced differences in the Jahn-Teller energies along the three crystal axes. The samples were glued to thread with a small amount of Duco cement, which may introduce small strains due to thermal-contraction differences. In addition, the minority phase may introduce both local strain and magnetic fields. It is also possible that there is some additional effect that is not accounted for by the theoretical model.

As can be seen from Fig. 5, the agreement between the theory and experiment is quite good with the concentration being the only adjustable parameter. However, one can ask whether a simpler theory would give equally good agreement. To this end, a fit to the magnetization data was also attempted for a crystal-field model alone.[22] This theory gives an anisotropy with decreasing magnitude for orientations along the (111), (110), and (100) directions, in agreement with the observed magnetic anisotropy. However, this model cannot explain the steep initial slope or the magnitude of the magnetization at 6 T with reasonable values of the concentration.

The fit was also attempted including the effects of a static Jahn-Teller distortion but ignoring corrections to the spin-orbit parameter due to mixing with the chemical bonds. A Jahn-Teller energy more than a factor of 3 below the measured value for E_{JT} was required to obtain

reasonable agreement with the data. This shows the shortcomings of the point-ion approximation for $Zn_{1-x}Cr_xTe$.

Another interesting question is whether a given Cr^{2+} ion is frozen into a single Jahn-Teller well—specifically can the Cr^{2+} ions relax preferentially into the lower-energy distortion sites perpendicular to the field? Magnetization measurements have been made on $Zn_{1-x}Cr_xSe$ and interpreted within such a picture.[12] Since the potential barrier between Jahn-Teller distortion sites is typically an order of magnitude smaller than the Jahn-Teller energy,[20] the barrier should be on the order of 40 cm^{-1}. Both thermal activation over and quantum tunneling through this barrier may occur.

The possibility for motion between states was explored for our samples by cooling in 0 T and observing the magnetization as a function of time after ramping to 6.0 T. On the time scale of hours, no drift that would indicate that the Cr^{2+} ions were relaxing to lower-energy distortions relative to the field axis was observed. A comparison of the data taken at 2.0 and at 5.4 K also showed very similar anisotropies. We might expect strong temperature-dependent effects if thermal activation over the barriers was important in this temperature range. Further, calculations were made to predict the magnetization as a function of field in the limit of free motion between states. We found the magnetization for this free tunneling regime leaves the (111) directions unaffected, as expected, but inverts the anisotropy so that the (100) direction has the largest magnetization. This is contradictory to the observed results. Therefore, we conclude that the transition rate between different Jahn-Teller distortions, if it occurs, must have a time scale longer than hours in our experiment and thus may be neglected.

Measurements of the magnetization vs temperature were also made at 1 T. After subtracting the constant diamagnetic and low-temperature ferromagnetic components, a plot of H/M vs T (Fig. 6) somewhat surprisingly shows a nearly straight line with a negative intercept typical of the Curie-Weiss behavior. Normally, a value for the effective nearest-neighbor exchange is extracted from this type of behavior. However, when the temperature dependence of the magnetization is calculated using the 25×25 Hamiltonian (plotted as a solid line in Fig. 6) and compared with the experimental results, the calculated temperature dependence shows good agreement with the experimental results, exhibiting even the curvature at low temperatures due to the reduced population of the excited states.

Below 4 K the data lie somewhat above the calculated values as can be seen in the inset of Fig. 6. One effect that is neglected in our analysis is the presence of nearest-neighbor pairs. In other DMS systems the nearest-neighbor interaction energy varies from 4 to around 50 K. Based on a random distribution, we would expect 4% of the Cr^{2+} ions would be nearest-neighbor pairs in our sample. If we simply assume that these Cr^{2+} ions are paired antiferromagnetically at our base temperature, they would no longer contribute to the magnetization. This would result in deviations of the observed magnitude. If this interpretation is correct then J_1/k_B would

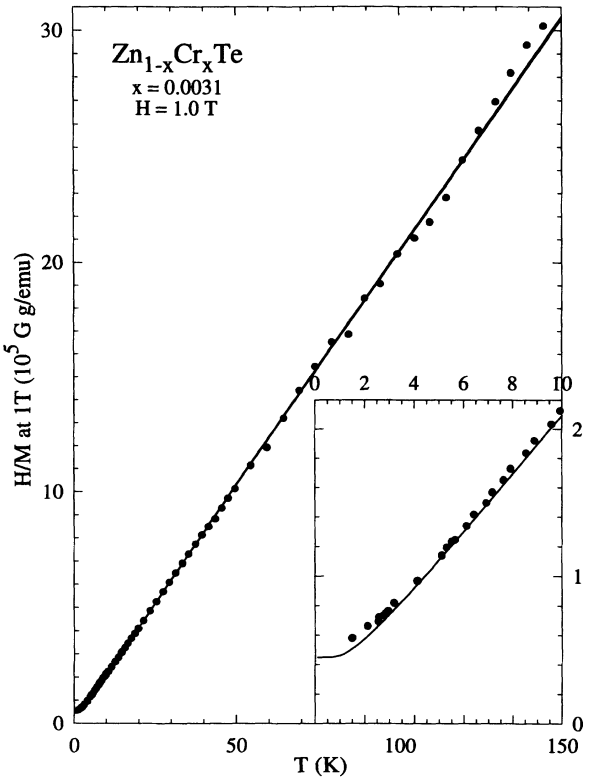

FIG. 6. H/M vs temperature for $Zn_{1-x}Cr_xTe$ for the (110) orientation. Note the saturation in M at low temperatures. The solid line is the theoretical prediction (110) direction. The inset shows the low-temperature behavior on an expanded scale.

be roughly equal to the temperature at which we observe deviations. We also note that the pair anisotropy is likely to be different from the single ion anisotropy, which may explain the small deviations seen in Fig. 5. Further work is needed to calculate the pair Hamiltonian and answer this question.

V. CONCLUSIONS

We have presented magnetization and heat-capacity data on $Zn_{1-x}Cr_xTe$. From our data we find that the ground state is a singlet, $m_s=0$, with a small splitting $D=3.1$ K to the doublet, $m_s=\pm1$, first excited state. The data is well described by a theory including a static Jahn-Teller distortion and ligand-field corrections. Agreement is obtained for theoretical parameters of $\Delta=4700$ cm^{-1}, $E_{JT}=320$ cm^{-1}, $\eta=V_2/V_1=0.294$, $\lambda_1=-59.4$ cm^{-1}, $\lambda_2=42.4$ cm^{-1}, $\rho_1=0.32$ cm^{-1}, $\rho_2=-0.09$ cm^{-1}, and $\rho_3=0.22$ cm^{-1}.

Above 1.5 K we observe additional heat capacity, which increases rapidly at higher temperatures. This is consistent with the presence of low-energy vibronic bands. On the other hand, we find no evidence for motion between the Jahn-Teller minima along the three crystal axes at temperatures up to 5.4 K in $Zn_{1-x}Cr_xTe$. This question requires further study in the Cr-based DMS's as nearly free motion was reported between the Jahn-Teller minimum in $Zn_{1-x}Cr_xSe$ (Ref. 12) at 2 K despite the fact that the Jahn-Teller energies are comparable.

ACKNOWLEDGMENTS

The authors wish to thank R. Sensemeier for his work on the AAS measurements; R. Colella, R. Eisenhower, and A. Mayer for their help orienting the crystals; and A. K. Ramdas, S. Rodriguez, and M. Villeret for very useful discussions. This work was supported by the National Science Foundation (NSF) under Material Research Group Grant No. DMR-922 139 0.

*Present address: Advanced Micro Devices, Inc., Austin, TX 78741.

[1]See, for example, *Diluted Magnetic Semiconductors,* edited by J. K. Furdyna and J. Kossut, Semiconductors and Semimetals Vol. 25 (Academic, Boston, 1988).

[2]J. T. Vallin, G. A. Slack, S. Roberts, and A. E. Hughes, Phys. Rev. B **2**, 4313 (1970).

[3]J. M. Langer and J. M. Baranowski, Phys. Status Solidi B **44**, 155 (1971).

[4]P. A. Slodowy and J. M. Baranowski, Phys. Status Solidi B **49**, 499 (1972).

[5]M. Kaminska, J. M Baranowski, S. M. Uba, and J. T. Vallin, J. Phys. C **12**, 2197 (1979).

[6]G. Grebe and H. J. Schulz, Z. Naturforsch. Teil A **29**, 1803 (1974).

[7]J. T. Vallin and G. D. Watkins, Phys. Rev. B **9**, 2051 (1974).

[8]J. Blinowski, P. Kacman, and H. Przybylinska, Solid State Commun. **79**, 1021 (1991).

[9]A. K. Bhattacharjee, Phys. Rev. B **46**, 5266 (1992).

[10]J. Blinowski and P. Kacman, Phys. Rev. B **46**, 12 298 (1992).

[11]A. K. Bhattacharjee, Phys. Rev. B **49**, 13 987 (1994).

[12]A. Twardowski, T. Fries, Y. Shapira, P. Eggenkamp. H. J. M. Swagten, and M. Demianiuk, J. Appl. Phys. **73**, 5745 (1993).

[13]W. Mac, Nguyen The Khoi, A. Twardowski, J. A. Gaj, and M. Demianiuk, Phys. Rev. Lett. **71**, 2327 (1993).

[14]J. M. Langer, C. Delerue, M. Lannoo, and H. Heinrich, Phys. Rev. B **38**, 7723 (1988).

[15]The coercive field, critical temperature, and saturation values suggest that approximately 12% of the Cr in the sample is present as CrTe.

[16]M Villeret, Ph.D. thesis, Purdue University, 1989.

[17]S. Rodriguez, *Encyclopedia of Applied Physics* (VCH, New York, 1993),Vol. 5, p. 431.

[18]J. S. Griffith, *The Theory of Transition Metal Ions* (Cambridge University Press , Cambridge, England, 1961).

[19]A. Abragam and B. Bleaney, *Electron Paramagnetic Resonance of Transition Ions* (Dover, New York, 1986).

[20]M. D. Sturge, in *Solid State Physics: Advances in Research and Applications,* edited by F. Seitz, D. Turnbull, and H. Ehrenreich (Academic, New York, 1967), Vol. 20, p. 91.

[21]G. Grebe, G. Roussos, and H.-J. Schulz, J. Lumin. **12/13**, 701 (1976).

[22]S. Rodriguez and M. Villeret, Phys. Rev. B **48**, 14 127 (1993).